Comparison of Two Phase Pressure Drop Models in 1-D Top Flooded Debris Bed

Mooneon Lee [a], Jin Ho Park [a], Eunho Kim [a], Hyun Sun Park [a*]
a Division of Advanced Nuclear Engineering, Pohang university of science and technology (POSTECH)
San 31, Hyoja-dong, Nam-gu, Pohang, Gyungbuk, Republic of Korea, 37673
[*]Corresponding author: hejsunny@postech.ac.kr

1. Introduction

In the very rare events of an accident in light water reactor (LWR), core melt down (so called severe accident) can possibly occur. When the accident progresses to the ex-vessel phase, the core material would be relocated into the containment. If the containment is flooded by water due to either leakage from cooling systems or severe accident management (SAM) measures, the relocated core material (called corium) would form particulate debris bed by fuel coolant interaction (FCI). Since the failure of containment would mean loss of the last barrier to protect public and environment from radioactive material release, the coolability of the particulate debris bed is one of crucial issues in the SAM of LWRs.

The dry out of coolant inside debris bed can be considered as the limitation of cooling in the conservative point of view and the heat flux through whole bed at the situation is named as Dryout Heat Flux (DHF). The modeling of DHF for debris bed started from early 1980s by several researchers[1-3]. It is known that DHF mainly occurs by hydrodynamic limitation inside porous media[4]. Therefore, there have been following attempts to capture flow resistance in porous media, precisely[5-7]. Up to date, although there are about seven pressure drop models[2, 3, 5-9] available in literatures, it is hard to find comparison of those models with a wide range of DHF experimental data.

The one attempt[9] was conducted in 2013, but due to lack of consideration of the capillary pressure in his work, the DHF values that he calculated seem to be underestimated, especially in the range of the small particle diameter cases.

In this research, the importance of capillary pressure in the comparison of pressure drop model with experimental data was checked and model selection among pressure drop models for the DHF calculation was also conducted.

2. Methods

General modeling approach used in this research is similar to the one used by Lipinski[1]. The following states are, in general, summary of his work. Some modifications to adopt several different pressure drop models are also commented.

2.1 Two phase pressure drop models in porous media

When the two fluid phases flow through porous media, the forces acting to each phase can be classified as gravity, drag with solid particles and interfacial drag force between two fluids.

The drag forces between solid particles and fluid in porous media can be written as below.

$$\overrightarrow{F_{pg}} = \varepsilon\alpha\left(\frac{\mu_g}{KK_{rg}}\overrightarrow{J_g} + \frac{\rho_g}{\eta\eta_{rg}}|\overrightarrow{J_g}|\overrightarrow{J_g}\right) \quad (1)$$

$$\overrightarrow{F_{pl}} = \varepsilon(1-\alpha)\left(\frac{\mu_l}{KK_{rl}}\overrightarrow{J_l} + \frac{\rho_l}{\eta\eta_{rl}}|\overrightarrow{J_l}|\overrightarrow{J_l}\right) \quad (2)$$

$$K = \frac{\varepsilon^3 d^2}{150(1-\varepsilon)^2} \quad (3)$$

$$\eta = \frac{\varepsilon^3 d}{1.75(1-\varepsilon)} \quad (4)$$

where ε is the porosity, α is the void fraction, μ is the viscosity, ρ is the density and $\vec{J}$ is the superficial velocity. K & η are the permeability and the passability, respectively and d is the particle diameter. K_r and η_r are the relative permeability and the relative passability, respectively, which are the model dependent parameters and the function of void fraction. The parameters for different models are summarized in Table I.

Table I: Relative permeability and passability in each model

Model	K_{rl}	η_{rl}	K_{rg}	η_{rg}
Reed[2]	$(1-\alpha)^3$	$(1-\alpha)^5$	α^3	α^5
Tung&Dhir[6]	$(1-\alpha)^4$	$(1-\alpha)^4$	$(\frac{1-\varepsilon}{1-\varepsilon\alpha})^{\frac{3}{4}}\alpha^m$	$(\frac{1-\varepsilon}{1-\varepsilon\alpha})^{\frac{3}{2}}\alpha^m$
Hu& Theofanous[3]	$(1-\alpha)^3$	$(1-\alpha)^6$	α^3	α^6
Schulenburg& Müller [8]	$(1-\alpha)^3$	$(1-\alpha)^5$	α^3	$\alpha^6\ (\alpha > 0.3)$ $0.1\alpha^4\ (else)$
Schmidt[5]	$(1-\alpha)^4$	$(1-\alpha)^4$	$(\frac{1-\varepsilon}{1-\varepsilon\alpha})^{\frac{3}{4}}\alpha^m$	$(\frac{1-\varepsilon}{1-\varepsilon\alpha})^{\frac{3}{2}}\alpha^m$
Rahman[7]	$(1-\alpha)^3$	$(1-\alpha)^6$	α^m	α^m
Yakush[9]	$(1-\alpha)^{2.4}$	$(1-\alpha)^5$	$\alpha^{2.4}$	α^5

The values of the power, m, in the Tung & Dhir model and the Schmidt and Rahman models vary between 3 and 4, depending on the two phase flow regimes.

The interfacial drag force between liquid and gas phases is considered only in some models. Summary of the interfacial drag forces are listed in Table II. As in the relative permeability and passability, the interfacial drag force in Tung & Dhir, Schmidt and Rahman model is somewhat complex due to its dependency on two phase flow regime. The details of their model can be found in literature[5-7].

With considering all forces mentioned above, the force balance equation in the 1-D steady state condition can be written as below

$$-\nabla p_g = \rho_g \vec{g} + \frac{\overrightarrow{F_{pg}}}{\varepsilon\alpha} + \frac{\vec{F_i}}{\varepsilon\alpha} \quad (5)$$

$$-\nabla p_l = \rho_l \vec{g} + \frac{\overrightarrow{F_{pl}}}{\varepsilon(1-\alpha)} - \frac{\vec{F_i}}{\varepsilon(1-\alpha)} \quad (6)$$

Table II: Interfacial drag forces

Model	F_i
Reed[2]	-
Tung&Dhir[6]	$A(\alpha)j_r + B(\alpha)\lvert j_r\rvert j_r$
Hu& Theofanous[3]	-
Schulenburg& Müller [8]	$C_1(1-\alpha)^7\alpha(\frac{j_g}{\alpha} - \frac{j_l}{1-\alpha})^2$, $C_1 = 350\frac{\rho_l K}{\eta\sigma}(\rho_l - \rho_g)g$
Schmidt[5]	$A(\alpha)j_r + B(\alpha)\lvert j_r\rvert j_r$
Rahman[7]	$A(\alpha)j_r + B(\alpha)\lvert j_r\rvert j_r$
Yakush[9]	-

2.2 Capillary pressure model

Leverett[10] found a relationship between the capillary pressure and the liquid saturation. He suggested a function of saturation, J(s), for this and is called the Leverett J function.

$$P_c = P_g - P_l = \sigma\cos\theta\sqrt{\frac{\varepsilon}{K}}J(s) \quad (7)$$

where σ is the surface tension and θ is the contact angle of liquid. And the saturation, s, equals to 1- α.

There are several options for J(s) in literature [1, 11, 12], but the later Lipinski model[11] has been used in this research.

$$J(s) = \frac{(\frac{1}{s}-1)^{0.3}}{\sqrt{5}} \quad (8)$$

2.3 Mass conservation

Under the assumption that all energy emitted from particles goes into the phase change of fluid, the steady state 1D mass conservation equations for each phase can be written as

$$\rho_g\frac{dj_g}{dz} = \Gamma \quad (9)$$

$$\rho_l\frac{dj_l}{dz} = W - \Gamma \quad (10)$$

where Γ and W are the evaporation rate and the liquid injection rate from bottom (kg/m^3s), respectively. By integration of the mass balance equations, the superficial velocity of each phase can be derived into

$$j_g = \frac{\ddot{q}z}{\rho_g\Delta H_{evap}} \quad (11)$$

$$j_l = w_r - \frac{\ddot{q}z}{\rho_l\Delta H_{evap}} \quad (12)$$

where $\ddot{q}$ is the volumetric heat generation (W/m^3), ΔH_{evap} is the latent heat (J/kg) and w_r is the water injection velocity (m/s). The heat flux, $\ddot{q}$ (W/m^2), is then defined as $\ddot{q}$ multiplied by height z(m).

2.4 Solution Procedure

If Eq. (5) is subtracted by Eq. (6), the left hand side becomes the gradient of the capillary pressure. Therefore, if it is combined with (7), the final equation becomes the first order ordinary differential equation(ODE) of the void fraction with the given heat flux.

$$\nabla p_g - \nabla p_l = \nabla p_c = (\rho_l - \rho_g)\vec{g} + \frac{\overrightarrow{F_{pl}}}{\varepsilon(1-\alpha)} - \frac{\overrightarrow{F_{pg}}}{\varepsilon\alpha} - (\frac{\vec{F_i}}{\varepsilon(1-\alpha)} + \frac{\vec{F_i}}{\varepsilon\alpha}) \quad (13)$$

For the boundary condition on the ODE, Lipinski & Reed suggested the channel region concept. In the concept, the length of channel region was proposed and the boundary value of saturation at the bottom of channeled region was given by either a correlation[1] or the constant of 0.99[2].

However, in this research, the channeling region is ignored and set the saturation value to 0.99 for the boundary condition at the top of debris bed. It is due to (1) the channeling concept has limitation for the model extension to multi-dimensional cases, which is the future work of this research, (2) ignorance of channel length does not show many difference and it will be discussed in section 3.2.

For the given heat flux and boundary conditions, Eq. (13) can be solved and the void fraction profile along the bed height can be achieved. For the determination of DHF, iterative calculations have to be conducted to obtained the heat flux until the void fraction becomes 1. During the calculation, the increment of the heat flux is 0.5% of the DHF value obtained from the Zero-D model without the capillary pressure consideration[13].

3. Results

3.1 Role of capillary pressure in the DHF modeling

To point out the improved accuracy of model comparison in this research comparing to the previous one[9], the effectiveness of the capillary pressure has been initially checked.

In general, the capillary pressure increases with smaller curvature of water droplet interfaces, the role of the capillary pressure, therefore, would be significantly enlarged with the smaller particle size. This can be easily seen from Fig. 1. Without calibration of any pressure drop model, the agreement of the DHF values between experimental data and model was significantly improved in the small particle size region.

In addition, the tendency of DHF increase with a smaller bed depth can only be captured by introducing the capillary pressure concept in the model as shown in Fig. 2.

It is because in the case of the lower bed height, the sharper void fraction profile would result in much stronger capillary pressure gradient as one can see from Eq. (3).

Therefore, for the comparison of the pressure drop model with the DHF experimental data, the consideration of the capillary pressure seems to play an important role.

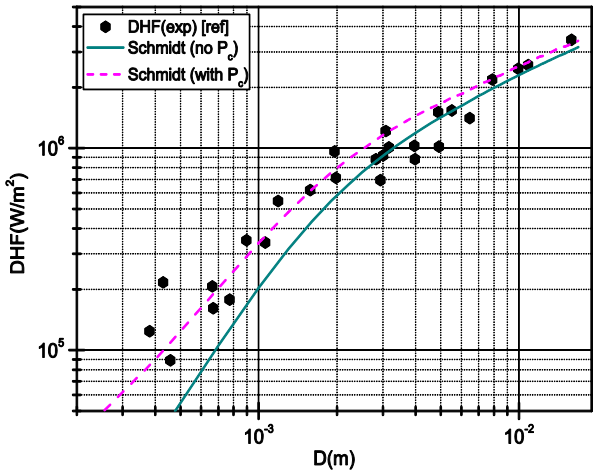

Fig 1. Capillary pressure effects in small particle region

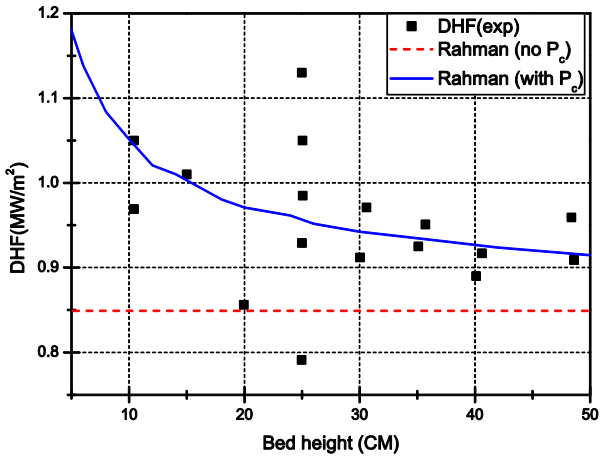

Fig 2. Hofmann's experiment[14] and capillary pressure effects.

3.2 Model comparison

The experimental data for DHF are collected from various literatures[14-19] for the cases of one dimensional configuration and the top flooding conditions. A total of number of experimental data is 108. The detailed condition ranges of each experiment are summarized in Table III.

The six pressure drop models used in the comparison and two more cases considered. The first case is the considering the channel length proposed by Reed, and the second one is the Reed model calibrated by Yakush[9].

Table IV shows the mean values with the standard deviations of error between experimental data and DHF results from models. It is obvious that the channeling effects show only minor effects on the error. The average of error was slightly improved with the channeling concept, but the standard deviation slightly increases as well. The calibrated Reed model proposed by Yakush shows slightly lower median value than the original Reed model does but it also has bigger standard deviation.

Table III: Experimental conditions

	Coolant	P (bar)	D(mm)	ε	Bed H(CM)
Barleon[15]	Water, Freon	1	2-15.88	0.386-0.473	2-41
Trenberth[16]	Water	1	1.2-2	0.368-0.45	2-14.3
Hofmann[14]	Water	1	3	0.405	10-48.6
POMECO[17]	Water	1	1.5-3	0.363-0.367	61
STYX[18]	Water	2.15-7	0.804	0.37	60
DEBRIS[19]	Water	1-5	2.8	0.37	64

Table IV: Mean and standard deviation of error

	Mean of error (%)	STD of error (%)
Reed (no channeling)	-4.00	21.71
Reed (with channeling)	-3.72	22.42
Tung & Dhir	-31.60	12.17
Hu & Theofanous	-26.01	17.75
Schulenburg & Müller	-16.56	22.65
Schmidt	0.96	19.19
Rahman	-7.78	20.67
Yakush	1.75	24.49

Over all, the Schmidt model seems to be the best fit for the experiments as it has the lowest mean of error and relatively smaller standard deviation. The probability to calculate the DHF value within $\pm 10\%$ and $\pm 20\%$ of errors in each model have been calculated by either histogram or normal distribution function of errors using its mean and standard deviation. In this case, Tung & Dhir, Hu & Theofanous, Schulenburg models have not been considered as their mean error values are over 10%, which are considerably larger than others.

As one can see in Table V, in general, all of models show quite similar results regardless of methods, which are the histogram and normal distribution function. As shown in Fig. 3, although it does not show the perfect normal distribution, it can be possibly assumed to be the normal distribution function.

The Yakush's calibrated model shows similar but a little bit of less accuracy to the original Reed model. It is probably overestimation of DHF in the small particle cases.

Overall, Schmidt model shows highest probability, but there are no significant differences between those four models.

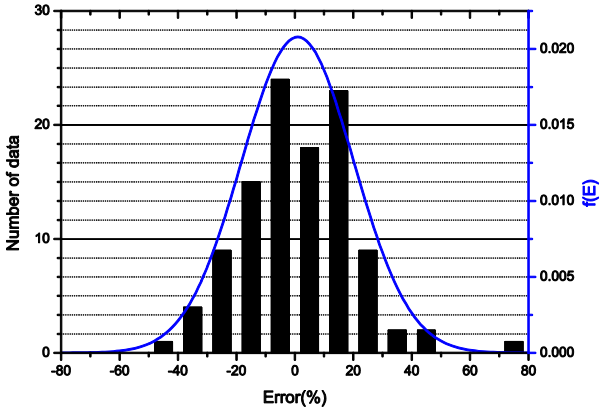

Fig. 3. Histogram and normal distribution of an error in Schmidt model.

Table V: Probability with regarding error range

	Histogram		Normal Distribution	
	±10%	±20%	±10%	±20%
Reed	35.2%	63.0%	34.9%	63.7%
Schmidt	38.9%	74.1%	39.7%	70.1%
Rahman	46.3%	64.8%	34.9%	63.2%
Yakush	19.4%	62.0%	31.8%	58.7%

4. Conclusions

The effectiveness of the capillary pressure on the DHF modeling has been examined in this study. The capillary pressure increases DHF especially for the smaller particle size and the shorter bed height since the capillary pressure increases with the smaller curvature of two phase interfaces, which is strongly related to the particle size, and the shorter bed height makes the sharper void fraction gradient resulting larger pressure gradient in a porous media.

The model comparison with 108 experimental data from various conditions has been conducted and the Schmidt model shows the best agreement to the experimental data although Reed, Rahman model also show similar results.

For the pressure drop model selection of multi-dimensional CFD simulation, since the co-current flow effects also should to be considered, additional work with the bottom-fed and multi-dimensional experimental data should also be conducted in near future.

ACKNOWLEDGEMENTS

This work was supported by the Nuclear Safety Research Program through the Korea Foundation Of Nuclear Safety(KOFONS), granted financial resource from the Nuclear Safety and Security Commission(NSSC), Republic of Korea (No. 1305008)

REFERENCES

[1] Lipinski, R.J., Model for boiling and dryout in particle beds.[LMFBR]. 1982, Sandia National Labs., Albuquerque, NM (USA).
[2] Reed, A.W., The effect of channeling on the dryout of heated particulate beds immersed in a liquid pool. 1982, Massachusetts Institute of Technology.
[3] Hu, K. and T. Theofanous, On the measurement and mechanism of dryout in volumetrically heated coarse particle beds. International journal of multiphase flow, 1991. 17(4): p. 519-532.
[4] Bürger, M., et al., Validation and application of the WABE code: Investigations of constitutive laws and 2D effects on debris coolability. Nuclear engineering and design, 2006. 236(19): p. 2164-2188.
[5] Schmidt, W., Interfacial drag of two-phase flow in porous media. International journal of multiphase flow, 2007. 33(6): p. 638-657.
[6] Tung, V. and V. Dhir, A hydrodynamic model for two-phase flow through porous media. International journal of multiphase flow, 1988. 14(1): p. 47-65.
[7] Rahman, S., Coolability of corium debris under severe accident conditions in light water reactors. 2013.
[8] Schulenberg, T. and U. Müller, An improved model for two-phase flow through beds of coarse particles. International journal of multiphase flow, 1987. 13(1): p. 87-97.
[9] Yakush, S., P. Kudinov, and N. Lubchenko, Coolability of heat-releasing debris bed. Part 1: Sensitivity analysis and model calibration. Annals of Nuclear Energy, 2013. 52: p. 59-71.
[10] Leverett, M., Capillary behavior in porous solids. Transactions of the AIME, 1941. 142(01): p. 152-169.
[11] Lipinski, R., A review of debris coolability models, in Light water reactor severe accident evaluation. 1983.
[12] Turland, B. and K. Moore, One-dimensional models of boiling and dryout, in Post accident debris cooling. 1983.
[13] Lee, M., J.H. Park, and H.S. Park, Validation of CFD Modeling for Multi-dimensional Effects in Ex-vessel Debris Bed Coolability, in Korean Nucelar Society Autumm Meeting. 2015: Gyeongju, Korea.
[14] Hofmann, G., On the location and mechanisms of dryout in top-fed and bottom-fed particulate beds. Nuclear Technology, 1984. 65(1): p. 36-45.
[15] Barleon, L., K. Thomauske, and H. Werle, Cooling of debris beds. Nuclear technology, 1984. 65(1): p. 67-86.
[16] Trenberth, R. and G. Stevens, An experimental study of boiling heat transfer and dryout in heated particulate beds. 1980, UKAEA Atomic Energy Establishment.
[17] Thakre, S., L. Li, and W. Ma, An experimental study on coolability of a particulate bed with radial stratification or triangular shape. Nuclear Engineering and Design, 2014. 276: p. 54-63.
[18] Lindholm, I., et al., Dryout heat flux experiments with deep heterogeneous particle bed. Nuclear engineering and design, 2006. 236(19): p. 2060-2074.
[19] Rashid, M., et al., Experimental results on the coolability of a debris bed with multidimensional cooling effects. Nuclear Engineering and Design, 2011. 241(11): p. 4537-4543.